

Excluded volume induces buckling in optically driven colloidal rings

Eric Cereceda-López ^{1,2,*} Mattia Ostinato ^{1,3,*} Antonio Ortiz-Ambriz ^{1,4} Arthur V. Straube ^{5,6,†}
Matteo Palassini ^{1,3} and Pietro Tierno ^{1,3,2,‡}

¹Departament de Física de la Matèria Condensada, Universitat de Barcelona, 08028 Barcelona, Spain

²Institut de Nanociència i Nanotecnologia, Universitat de Barcelona, 08028 Barcelona, Spain

³Universitat de Barcelona Institute of Complex Systems (UBICS), Universitat de Barcelona, 08028 Barcelona, Spain

⁴Tecnologico de Monterrey, Escuela de Ingeniería y Ciencias, Monterrey 64849, Mexico

⁵Zuse Institute Berlin, Takustraße 7, 14195 Berlin, Germany

⁶Freie Universität Berlin, Department of Mathematics and Computer Science, Arnimallee 6, 14195 Berlin, Germany



(Received 27 July 2023; accepted 21 December 2023; published 1 March 2024)

In our combined experimental, theoretical, and numerical work, we study the out-of-equilibrium deformations in a shrinking ring of optically trapped, interacting colloidal particles. Steerable optical tweezers are used to confine dielectric microparticles along a circle of discrete harmonic potential wells, and to reduce the ring radius at a controlled quench speed. We show that excluded-volume interactions are enough to induce particle sliding from their equilibrium positions and nonequilibrium zigzag roughening of the colloidal structure. Our work unveils the underlying mechanism of interfacial deformation in radially driven microscopic discrete rings.

DOI: [10.1103/PhysRevResearch.6.L012044](https://doi.org/10.1103/PhysRevResearch.6.L012044)

Introduction. Surface roughening occurs in a wide variety of physical [1,2] and biological systems [3–5] and it is often caused by noise or external perturbations which deform an initially flat and spatially uniform interface [6,7]. Such a process has received much attention on extended systems, i.e., when macroscopically large domains grow and deform, including fluid [8–11] and solid [12–15] interfaces, grain boundaries [16–18], or active matter [19–21]. However, finite-size systems made of expanding or shrinking circular domains also show kinetic roughening when driven out of equilibrium by internal fluctuations or pressure imbalance. Physical examples include unilamellar vesicles [22,23], confined bacteria colonies [24,25], nematic liquid-crystal droplets [26,27], or self-avoiding ring polymers [28,29]. In most of the cases, interfacial deformations are described with continuum models based on stochastic differential equations, such as the celebrated Kardar-Parisi-Zhang equation [2] or more sophisticated theories [30,31]. An alternative, although less exploited approach consists in considering the microscopic constituent of an interface, to understand how the global deformation arises directly from their pair interactions. Few works along this direction showed that spherical [32] or anisotropic [33] particles can indeed act as a microscopic model system for interfacial deformations.

When two colloidal particles approach each other, they interact due to long-range electrostatic [34] or hydrodynamic [35–39] forces or short-range steric effects arising from adsorbed polymer layers [40]. However, when brought at very close contact, a strong repulsion emerges from the excluded volume, namely the mutual particle impenetrability. While such an effect is negligible at extreme particle dilution, it strongly affects the diffusion [41–43], transport [44–47], and rheological [48,49] properties of dense colloidal suspensions. Excluded volume creates geometrically frustrated buckled systems under strong confinement [50,51], or it can be used to engineer novel colloidal phases and structures [52,53]. Further on, excluded-volume interactions go beyond the colloidal domain, being determinant in many granular [54,55], polymeric [56,57], or biological [58,59] systems.

Many studies on colloidal particles confined to a ring have focused on the particle displacement along the *tangential* direction, keeping fixed the radius of the ring [35–39]. Recently, this setup has shown striking effects as the emergence of propagating cluster defects [47,60] when compared to other related discrete systems based on linear, nearest-neighbor coupling [61]. In contrast, here we investigate the much less studied mechanism of out-of-equilibrium deformations induced by *radially* shrinking a ring of discrete particles at different compression speeds. We exploit the synergy between the experiment, theory and numerical simulations to show that buckling predominantly arises from excluded volume, without the need to consider long-range interactions, such as e.g. dipolar, electrostatic or hydrodynamic forces. Unlike roughening induced by thermal fluctuations in presence of dipolar interactions [32], the well-controlled quench speed becomes a key driving factor that determines driven buckling.

Experiments. Our colloidal ring of radius R is composed of $N = 50$ polystyrene particles having $d = 4.0 \mu\text{m}$

*These authors equally contributed to this work.

†straube@zib.de

‡ptierno@ub.edu

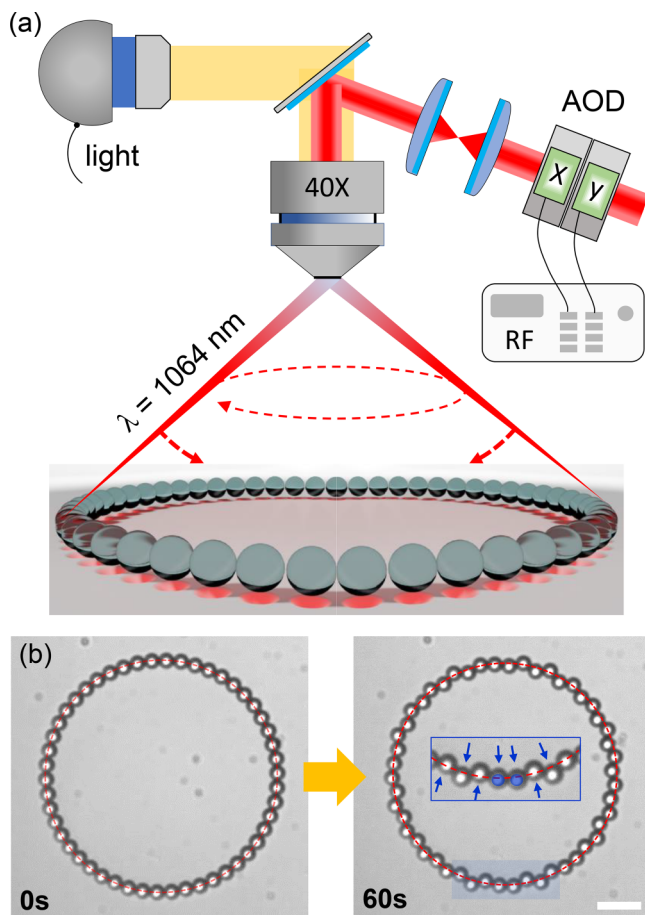


FIG. 1. Schematic of the experimental system: One infrared laser beam is rapidly steered via a two-channel (x, y) acousto-optic deflector (AOD) controlled via a radio-frequency generator (rf). The laser is scanned across equispaced points forming a ring of quasistatic double wells. (b) Two images showing the roughening of $N = 50$ polystyrene particles when the optical ring is reduced from $R(0) = 33.0 \mu\text{m}$ (left) to $R(\tau_q) = 31.0 \mu\text{m}$ (right) at a speed of $v_q = 0.06 \mu\text{m s}^{-1}$ (quench time $\tau_q = 60 \text{ s}$). Small arrows in the inset of the right image indicate displaced particles, with one central defect highlighted. The dashed red line is the ring circumference [see also Video S1 in the Supplemental Material (SM) [62]].

diameter, dispersed in highly de-ionized water (MilliQ, Millipore). The particle solution is placed by capillarity inside a thin ($\sim 100 \mu\text{m}$) chamber made of a borosilicate glass slide and a coverslip separated with a layer of parafilm. The experiments are performed at the room temperature of $T = 293 \text{ K}$. We trap the particles using time-shared optical tweezers which are created by passing an infrared laser beam (ManLight ML5-CW-P/TKS-OTS operating at 3 W, wavelength $\lambda = 1064 \text{ nm}$) through a pair of acousto-optic deflectors (AODs, AA Optoelectronics DTSXY-400-1064) both driven and synchronized with a radio-frequency (rf) generator (DDSPA2X-D431b-34). The beam is then focused from above by a microscope objective (Nikon 40 \times CFI APO) [Fig. 1(a)]. The bottom of the experimental chamber is observed with a second microscope objective (Nikon 40 \times Plan Fluor) which projects an image onto a complementary metal-oxide semiconductor camera (Ximea MQ003MG-CM), in a custom-built

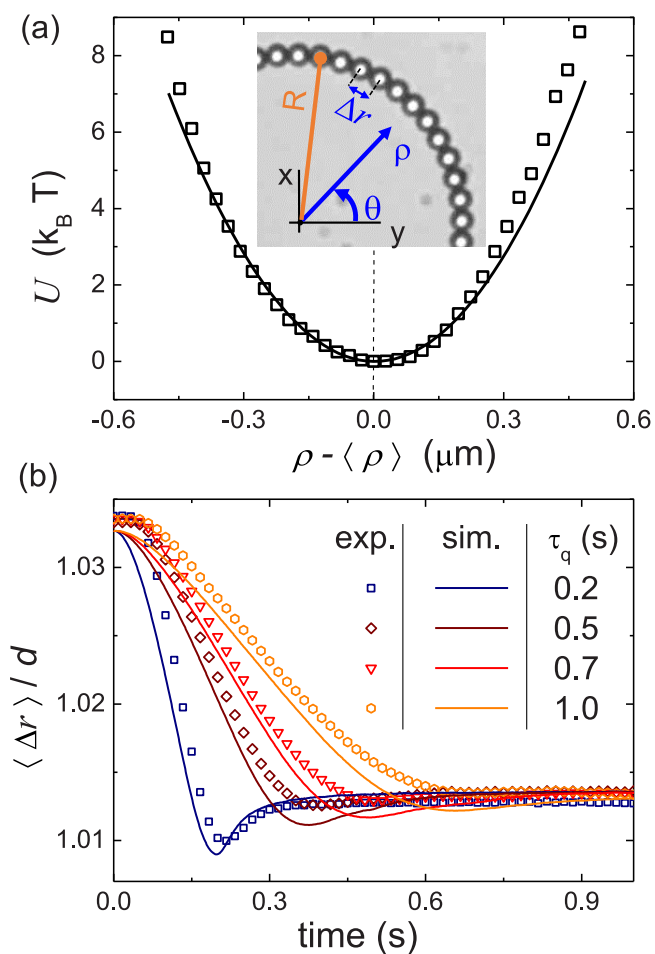


FIG. 2. (a) Confining potential $U(\rho)$ along the radial (ρ) direction calculated from the particle fluctuations before compression, where $\langle \rho \rangle = 33.0 \mu\text{m}$. Scattered squares are experimental data, and the continuous line is a nonlinear regression calculating $U(\rho)$ from Eq. (1). The inset shows a colloidal ring with highlighted Cartesian (x, y) and polar (ρ, θ) coordinate systems, with Δr the nearest-neighbor distance between the centers of the particles along the ring. (b) Average distance between the centers of nearest-neighbor particles $\langle \Delta r \rangle$ vs time for four different quench times τ_q from experiments (symbols) and simulations (lines).

inverted optical microscope. The laser tweezers visit 50 equispaced positions along a ring, spending $20 \mu\text{s}$ in each position, such that each trap is visited once every $\sim 1 \text{ ms}$. Thus, the potential wells can be considered as quasistatic since the beam scanning is much faster than the typical self-diffusion time of the particles, $\tau_D = d^2/(4D_{\text{eff}}) \sim 30 \text{ s}$, estimated from the effective particle diffusion coefficient $D_{\text{eff}} \simeq 0.13 \mu\text{m}^2 \text{ s}^{-1}$ [39].

Ring deformation. We start by analyzing the optical potential confining the colloidal particles within a ring of mean radius $33.0 \mu\text{m}$. As shown in the inset in Fig. 2(a), we work in polar coordinates with the origin at the center of the ring. Before compression, we determine the spring constant κ of the optical potential confining each particle by monitoring the equilibrium, radial particle fluctuations across the ring. One can obtain the confining potential $U(\mathbf{r})$ by measuring the stationary probability distribution directly from the particle trajectories [63]. To adapt such a procedure to the radial

configuration, we formulate the overdamped equation of motion for an individual Brownian particle with the position $\mathbf{r} = (x, y)$ captured in a radial harmonic trap centered at \mathbf{R} (with $|\mathbf{R}| = R$), $\gamma\dot{\mathbf{r}} = -\kappa(\mathbf{r} - \mathbf{R}) + \xi$, where κ is the trap stiffness, $\gamma = 3\pi\eta d$ the drag coefficient of the particle, η the viscosity of water, and ξ a stochastic force with zero average and delta correlated. The corresponding stationary distribution of the particle position is $P(\mathbf{r}) \propto \exp[-U(\mathbf{r})/k_B T]$, where $U(\mathbf{r}) = \kappa(\mathbf{r} - \mathbf{R})^2/2$. Passing to polar coordinates for $(\rho = |\mathbf{r}|, \theta)$ and making use of the radial symmetry of $P(\mathbf{r})$, we integrate over θ to find that the stationary distribution of the radial displacement has the ‘‘Rayleigh’’ form,

$$P(\rho) = C\rho e^{-U(\rho)/k_B T}, \quad U(\rho) = \frac{\kappa}{2}(\rho - R)^2, \quad (1)$$

with C being the normalization constant. For details, see the Supplemental Material (SM) [62]. We invert Eq. (1) as $U(\rho) = -k_B T \ln\{RP(\rho)/[\rho P(R)]\}$ and calculate the radial potential from the experimentally determined displacement distribution. Figure 2(a) shows the experimental data (open squares) with a nonlinear regression using the expression in Eq. (1) for $U(\rho)$. From these data we extract the optical spring constant $\kappa = (2.51 \pm 0.02) \times 10^{-4}$ pN nm $^{-1}$.

In a typical shrinking experiment [Fig. 1(b)], we first equilibrate the trapped particles along a ring with an initial radius $R(t=0) = 33.0$ μm . After that, we perform 50 measuring cycles by repeatedly decreasing the radius to $R(t=\tau_q) = 31.0$ μm at a controlled quench speed $v_q = [R(0) - R(\tau_q)]/\tau_q$ and, after a short equilibration period, increasing it back to its initial position. The experiments run over 24 h during which we change the quench time $\tau_q \in [0.2, 10]$ s and speed $v_q \in [0.37, 18.5]$ $\mu\text{m s}^{-1}$ ensuring the same statistical averages for each value of τ_q .

At $t=0$, the particles lay almost along their mean elevation $\langle \rho_i \rangle \approx R$, with a small thermal roughening $W(t=0) = W_0$ induced by thermal fluctuations, where we define the roughening $W(t)$ as

$$W^2(t) = \frac{1}{N} \sum_i \langle h_i^2(t) \rangle, \quad (2)$$

in which $h_i = \rho_i - \langle \rho_i \rangle$ is the radial displacement of particle i ($=1, \dots, N$) from the mean.

Upon decreasing the ring radius, the colloids start interacting and excluded volume displaces the particles either outside or inside the ring. For the chosen number of particles, the ground state of the system would be a perfect zigzag chain with no defects [64], which could be obtained for an adiabatically slow compression, $\tau_q \rightarrow \infty$. However, at a finite quench time defects in the zig-zag configuration emerge in the form of two or more particles displaced together [inset in Fig. 1(b)]. The effect of excluded-volume interactions can already be appreciated by measuring the evolution of the average distance $\langle \Delta r \rangle$ between the centers of neighboring particles [Fig. 2(b)]. For the fastest compression occurring at $\tau_q = 0.2$ s, $\langle \Delta r \rangle$ displays a pronounced minimum close to the excluded-volume limit, $\langle \Delta r \rangle = d$, indicating a strong repulsive force around $t \sim \tau_q$. After that, the particles reach a steady distance of $\langle \Delta r \rangle \sim 1.013d$, regardless of the compression time. Reducing the compression speed gradually eliminates this minimum since the slower approach allows the colloids to

rearrange, sliding out from their central position in the harmonic wells.

Numerical simulations. To understand whether the induced buckling can be described by only taking into account excluded-volume interactions, we perform Brownian dynamics simulations with the same parameters as in the experiments. We extend our single-particle description to many interacting particles, in which each particle i obeys the Langevin equation

$$\gamma\dot{\mathbf{r}}_i = -\kappa(\mathbf{r}_i - \mathbf{R}_i) + \mathbf{f}_{i,i+1} + \mathbf{f}_{i,i-1} + \xi_i, \quad (3)$$

where the force $\mathbf{f}_{i,j} = -U'_{\text{HC}}(r_{ij})\mathbf{r}_{ij}/r_{ij}$ represents the hard-core repulsive interaction between nearest neighbors. To achieve the best mapping with the experimental data, we generalize the Weeks-Chandler-Andersen potential [65] as $U_{\text{HC}}(r) = 4\epsilon[(d/r)^{2q} - (d/r)^q + 1/4]$ for $r \leq r_0 = 2^{1/q}d$ and zero otherwise. Here, ϵ is the repulsion strength and q the nonlinearity index. As shown in Figs. 2(b) and 3(b), we find quantitative agreement between simulations and experiments by using $q = 42$ and $\epsilon/\gamma = 2.5$ $\mu\text{m}^2 \text{s}^{-1}$ as fitting parameters [62]. This matching highlights that the particles experience an effective short-range repulsive potential, a quantity frequently subject to uncertainty due to the presence of residual particle charges and long-range interactions. Further, by varying the number N of particles at constant τ_q , data not shown here, the roughening shows a similar crossover from the same thermal plateau W_0 at small times to the saturation limit W_S at long times. While W_S grows only slightly for larger N , it exhibits a stronger nonuniform decrease for smaller N , due to the nonlinear nature of the short-range interactions.

Theory. We introduce the following one-dimensional model for the radial displacements:

$$\gamma\dot{h}_i = -\kappa g(t)(h_{i+1} - 2h_i + h_{i-1}) - \kappa h_i + \xi_i. \quad (4)$$

Unlike a previous work on thermal-induced roughening of a linear chain [cf. Eq. (2) in Ref. [32]], our Eq. (4) goes beyond the nondriven framework, as it includes a time-dependent factor $g(t)$ that encapsulates the increase in the effective interactions as the ring is compressed. Moreover, the particle interactions considered here are repulsive [$g(t) > 0$], in contrast to Ref. [32].

Equation (4) can be justified by projecting Eq. (3) of the simulations onto the radial direction (see SM [62]). In this way we obtain $g(t) = 0$ for $t < t_c$ and $g(t) = 2q^2\epsilon[R_c/R(t) - 1]/(r_0^2\kappa)$ for $t > t_c$, where $R(t) = R(0) - v_q t$ is the ring radius at time t , and t_c is the time at which $R(t) = R_c \equiv Nr_0/2\pi$ and the particles start to interact. Note that in Eq. (4) we have omitted a term $D/(h_i + R)$, which is negligible for our experimental conditions [62].

Using the discrete Fourier transform, from Eq. (4) we calculate the equal-time height-height correlation function $C(k, t) = N^{-1} \sum_i \langle h_i(t) h_{i+k}(t) \rangle$ of the ring,

$$C(k, t) = 2(-1)^k D \int_{-t_{\text{eq}}}^t F_k(t, t') dt', \quad (5)$$

with $F_k(t, t') = I_k[(4/\tau_0) \int_{t'}^t g(s) ds] \exp[-2(t-t')/\tau_0 + (4/\tau_0) \int_{t'}^t g(s) ds]$. Here, $\tau_0 = \gamma/\kappa$ is the microscopic relaxation time, $I_k(x)$ is the modified Bessel function of the first kind, and t_{eq} is an equilibration time which we

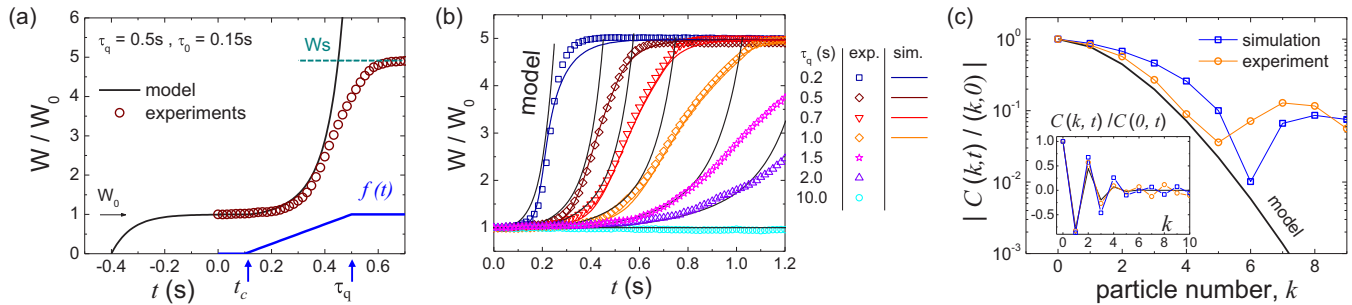


FIG. 3. (a) Normalized roughening, $W(t)/W_0$ vs t from experiments (symbols) and Eq. (6) (black line) for $\tau_q = 0.5$ s and $t_{\text{eq}} = 0.4$ s. The linear schedule $f(t)$ is shown in blue. (b) $W(t)/W_0$ vs t from experiments (symbols), simulations (lines in color), and the model (black line) for different τ_q . (c) Absolute value of the normalized, equal-time correlation function $C(k, t)/C(0, t)$ vs particle number k in logarithmic scale. Open symbols are experimental (circles) and simulation (squares) data for $\tau_q = 0.5$ s, while the continuous line is the numerical integration of Eq. (5) at time $t = 0.45$ s at which the predicted $W(t)$ reaches W_S . The bottom inset shows the correlations in normal scale.

suppose is much larger than τ_0 so that at $t = 0$ the system is in thermal equilibrium. For $k = 0$, we obtain the roughening [cf. Eq. (2)]:

$$W^2(t) = \frac{2W_0^2}{\tau_0} \int_{-t_{\text{eq}}}^t F_0(t, t') dt'. \quad (6)$$

In Eq. (6), we fix from the experimental data $\tau_0 = 0.15$ s and $W_0 = \sqrt{D_{\text{eff}}\tau_0} = 0.127$ μm which denotes the “thermal” roughening.

This equation predicts that, starting from $t = -t_{\text{eq}}$, $W(t)$ will first grow as $W(t) = W_0\{1 - \exp[-2(t + t_{\text{eq}})/\tau_0]\}$, as shown by the dashed line in Fig. 3(a), reach a thermal plateau W_0 for $-t_{\text{eq}} + \tau_0 \ll t \ll t_c$, and grow again for $t > t_c$ due to the repulsive interaction. For simplicity, we use a linear schedule $cf(t)$ that approximates well the full $g(t)$ [62], where $f(t) = 0$ for $t < t_c$, $(t - t_c)/(\tau_q - t_c)$ for $t_c \leq t \leq \tau_q$, and 1 for $t > \tau_q$. This schedule is shown by the blue line in Fig. 3(a). Here, c is a dimensionless constant which can be related to the pair interactions between the colloidal particles as $c = [1 - R(\tau_q)/R_c]2q^2\epsilon/(r_0^2\kappa)$.

Figure 3(b) shows the roughening from rings compressed at different $\tau_q \in [0.2, 10]$ s. We use Eq. (6) to fit the experimental data, the only adjustable parameters being t_c/τ_q and c . We obtain a good quantitative description of the initial increase of $W(t)/W_0$ at different τ_q by using $t_c/\tau_q = 0.2$ and $c = 0.9$, which determine $q = 10.7$ and $\epsilon/\gamma = 5.4$ $\mu\text{m}^2\text{s}^{-1}$, respectively. Note that both values differ only slightly from those for the full numerical model [Eq. (3)] despite a number of simplifications made to derive Eq. (4). Interestingly, for $c < 1/4$ the model is able to predict that $W(t)$ reaches an intrinsic saturation value $W_\infty = W_0(1 - 4c)^{-1/4}$ for $t \gg \tau_q$, whereas for $c > 1/4$ it grows without bounds, indicating that the particles escape from the optical traps. Note that the linear approximation for the short-range repulsion force in Eq. (4) is insufficient to describe the final stages of the compression, when the interaction becomes very large. Thus, the quantitative agreement with the saturation value W_S set by the experimental protocol can only be achieved by simulations. Note also that it is not possible to measure experimentally the initial growth until W_0 because the initial particle configuration in the ring is not perfectly flat.

Finally, we also use the model to contrast the experiments, theory and simulations in terms of the equal-time correlation function $C(k, t)$ [Fig. 3(c)]. For a fixed t , both experiments and simulations display anticorrelations in $C(k, t)$, as described by Eq. (5) [see the inset of Fig. 3(c)], which is a signature of the underlying zigzag pattern. The model fits rather well the experimentally determined correlation function up to a distance $k = 5$ particles. Above this range, the data start deviating and both simulations and experiments display a series of oscillations that may be due to the correlated lateral displacement of the particles, which are not considered by our theory.

Conclusions. We have used a colloidal model system to investigate the deformations emerging from a collapsing chain of optically driven microscopic particles. Via a tight combination of experiments, theory, and simulations, we find that nonequilibrium buckling is captured quantitatively well by considering the sole excluded-volume interactions, thus without any long-range dipolar, electrostatic, steric (polymer-mediated), or hydrodynamic effects. Different works have investigated the effect of topology on the collapse of a dried dense colloidal suspension [66–69]. Here, we have focused on the mechanism leading to buckling starting from the interparticle interactions. We expect that our general description of a finite shrinking ring at the discrete, i.e., single-particle level, may be important to related research fields where finite droplets reduce and deform due to external or internal (i.e., active) pressure fields.

Acknowledgments. We acknowledge stimulating discussions with Thomas M. Fischer, Hartmut Löwen, and Adolfo del Campo. This project has received funding from the European Research Council (ERC) under the European Union’s Horizon 2020 research and innovation programme (Grant Agreement No. 811234). A.V.S. acknowledges support by the Deutsche Forschungsgemeinschaft (DFG) under Germany’s Excellence Strategy-MATH+: The Berlin Mathematics Research Center (EXC-2046/1)-Project No. 390685689 (Subproject AA1-18). M.P. acknowledges support by Agència de Gestió d’Ajuts Universitaris i de Recerca (AGAUR) (No. 2021 SGR 00247) and Agència Estatal de Investigació (MINECO) (No. PID2022-139913NB-I00). P.T. acknowledge support the Generalitat de Catalunya under Program “ICREA Acadèmia” and AGAUR (No. 2021 SGR 00450).

- [1] S. T. Chui and J. D. Weeks, Dynamics of the roughening transition, *Phys. Rev. Lett.* **40**, 733 (1978).
- [2] M. Kardar, G. Parisi, and Y.-C. Zhang, Dynamic scaling of growing interfaces, *Phys. Rev. Lett.* **56**, 889 (1986).
- [3] T. Vicsek, M. Cserző, and V. K. Horváth, Self-affine growth of bacterial colonies, *Physica A* **167**, 315 (1990).
- [4] J. I. Wakita, H. Itoh, T. Matsuyama, and M. Matsushita, Self-affinity for the growing interface of bacterial colonies, *J. Phys. Soc. Jpn.* **66**, 67 (1997).
- [5] G. Rapin, N. Caballero, I. Gaponenko, B. Ziegler, A. Rawleigh, E. Moriggi, T. Giamarchi, S. A. Brown, and P. Paruch, Roughness and dynamics of proliferating cell fronts as a probe of cell-cell interactions, *Sci. Rep.* **11**, 8869 (2021).
- [6] T. Vicsek, *Fractal Growth Phenomena* (World Scientific, Singapore, 1992).
- [7] A.-L. Barabási and H. E. Stanley, *Fractal Concepts in Surface Growth* (Cambridge University Press, Cambridge, UK, 1995).
- [8] E. G. Flekkøy and D. H. Rothman, Fluctuating fluid interfaces, *Phys. Rev. Lett.* **75**, 260 (1995).
- [9] F. W. Starr, S. T. Harrington, B. M. Boghosian, and H. E. Stanley, Interface roughening in a hydrodynamic lattice-gas model with surfactant, *Phys. Rev. Lett.* **77**, 3363 (1996).
- [10] D. Stelitano and D. H. Rothman, Fluctuations of elastic interfaces in fluids: Theory, lattice-boltzmann model, and simulation, *Phys. Rev. E* **62**, 6667 (2000).
- [11] L. M. C. Sagis, Fluctuations of permeable interfaces in water-in-water emulsions, *Phys. Rev. Lett.* **98**, 066105 (2007).
- [12] H. van Beijeren, Exactly solvable model for the roughening transition of a crystal surface, *Phys. Rev. Lett.* **38**, 993 (1977).
- [13] M. S. Hoogeman, M. A. J. Kliik, D. C. Schlöber, L. Kuipers, and J. W. M. Frenken, Real-space measurement of surface roughening, *Phys. Rev. Lett.* **82**, 1728 (1999).
- [14] H. P. Bonzel, 3D equilibrium crystal shapes in the new light of STM and AFM, *Phys. Rep.* **385**, 1 (2003).
- [15] S. Balibar, H. Alles, and A. Y. Parshin, The surface of helium crystals, *Rev. Mod. Phys.* **77**, 317 (2005).
- [16] S. Gokhale, K. H. Nagamanasa, V. Santhosh, A. K. Sood, and R. Ganapathy, Directional grain growth from anisotropic kinetic roughening of grain boundaries in sheared colloidal crystals, *Proc. Natl. Acad. Sci. USA* **109**, 20314 (2012).
- [17] F. A. Lavergne, D. G. A. L. Aarts, and R. P. A. Dullens, Anomalous grain growth in a polycrystalline monolayer of colloidal hard spheres, *Phys. Rev. X* **7**, 041064 (2017).
- [18] M. Liao, X. Xiao, S. T. Chui, and Y. Han, Grain-boundary roughening in colloidal crystals, *Phys. Rev. X* **8**, 021045 (2018).
- [19] T. Andac, P. Weigmann, S. K. P. Velu, E. Pince, G. Volpe, G. Volpe, and A. Callegari, Active matter alters the growth dynamics of coffee rings, *Soft Matter* **15**, 1488 (2019).
- [20] G. Fausti, E. Tjhung, M. E. Cates, and C. Nardini, Capillary interfacial tension in active phase separation, *Phys. Rev. Lett.* **127**, 068001 (2021).
- [21] B. Lemma, N. P. Mitchell, R. Subramanian, D. J. Needleman, and Z. Dogic, Active microphase separation in mixtures of microtubules and tip-accumulating molecular motors, *Phys. Rev. X* **12**, 031006 (2022).
- [22] J. Pécéréaux, H.-G. Döbereiner, J. Prost, J.-F. Joanny, and P. Bassereau, Refined contour analysis of giant unilamellar vesicles, *Eur. Phys. J. E* **13**, 277 (2004).
- [23] M. D. El Alaoui Faris, D. Lacoste, J. Pécéréaux, J.-F. Joanny, J. Prost, and P. Bassereau, Membrane tension lowering induced by protein activity, *Phys. Rev. Lett.* **102**, 038102 (2009).
- [24] M. A. C. Huergo, M. A. Pasquale, P. H. González, A. E. Bolzán, and A. J. Arvia, Dynamics and morphology characteristics of cell colonies with radially spreading growth fronts, *Phys. Rev. E* **84**, 021917 (2011).
- [25] Z. You, D. J. G. Pearce, A. Sengupta, and L. Giomi, Mono- to multilayer transition in growing bacterial colonies, *Phys. Rev. Lett.* **123**, 178001 (2019).
- [26] K. A. Takeuchi and M. Sano, Universal fluctuations of growing interfaces: Evidence in turbulent liquid crystals, *Phys. Rev. Lett.* **104**, 230601 (2010).
- [27] K. A. Takeuchi, M. Sano, T. Sasamoto, and H. Spohn, Growing interfaces uncover universal fluctuations behind scale invariance, *Sci. Rep.* **1**, 34 (2011).
- [28] G. Witz, K. Rechendorff, J. Adamcik, and G. Dietler, Conformation of ring polymers in 2D constrained environments, *Phys. Rev. Lett.* **106**, 248301 (2011).
- [29] S. N. Santalla, J. Rodríguez-Laguna, and R. Cuerno, Circular Kardar-Parisi-Zhang equation as an inflating, self-avoiding ring polymer, *Phys. Rev. E* **89**, 010401(R) (2014).
- [30] T. Halpin-Healy and Y.-C. Zhang, Kinetic roughening phenomena, stochastic growth, directed polymers and all that. Aspects of multidisciplinary statistical mechanics, *Phys. Rep.* **254**, 215 (1995).
- [31] J. Krug, Origins of scale invariance in growth processes, *Adv. Phys.* **254**, 139 (2006).
- [32] R. Toussaint, G. Helgesen, and E. G. Flekkøy, Dynamic roughening and fluctuations of dipolar chains, *Phys. Rev. Lett.* **93**, 108304 (2004).
- [33] P. J. Yunker, M. A. Lohr, T. Still, A. Borodin, D. J. Durian, and A. G. Yodh, Effects of particle shape on growth dynamics at edges of evaporating drops of colloidal suspensions, *Phys. Rev. Lett.* **110**, 035501 (2013).
- [34] W. B. Russel, D. A. Saville, and W. R. Schowalter, *Colloidal Dispersions* (Cambridge University Press, Cambridge, UK, 1989).
- [35] C. Lutz, M. Reichert, H. Stark, and C. Bechinger, Surmounting barriers: The benefit of hydrodynamic interactions, *Europhys. Lett.* **74**, 719 (2006).
- [36] Y. Roichman, D. G. Grier, and G. Zaslavsky, Anomalous collective dynamics in optically driven colloidal rings, *Phys. Rev. E* **75**, 020401(R) (2007).
- [37] Y. Sokolov, D. Frydel, D. G. Grier, H. Diamant, and Y. Roichman, Hydrodynamic pair attractions between driven colloidal particles, *Phys. Rev. Lett.* **107**, 158302 (2011).
- [38] H. Nagar and Y. Roichman, Collective excitations of hydrodynamically coupled driven colloidal particles, *Phys. Rev. E* **90**, 042302 (2014).
- [39] D. Lips, E. C.-L. A. Ortiz-Ambroz, P. Tierno, A. Ryabov, and P. Maass, Hydrodynamic interactions hinder transport of flow-driven colloidal particles, *Soft Matter* **18**, 8983 (2022).
- [40] E. B. Zhulina, O. V. Borisov, and V. A. Priamitsyn, Theory of steric stabilization of colloid dispersions by grafted polymers, *J. Colloid Interface Sci.* **137**, 495 (1990).
- [41] J. Dzubiella, H. Löwen, and C. N. Likos, Depletion forces in nonequilibrium, *Phys. Rev. Lett.* **91**, 248301 (2003).
- [42] M. Bruna and S. J. Chapman, Excluded-volume effects in the diffusion of hard spheres, *Phys. Rev. E* **85**, 011103 (2012).

- [43] F. Rusciano, R. Pastore, and F. Greco, Fickian non-gaussian diffusion in glass-forming liquids, *Phys. Rev. Lett.* **128**, 168001 (2022).
- [44] W. K. Kegel and A. van Blaaderen, Direct observation of dynamical heterogeneities in colloidal hard-sphere suspensions, *Science* **287**, 290 (2000).
- [45] D. Lips, A. Ryabov, and P. Maass, Brownian asymmetric simple exclusion process, *Phys. Rev. Lett.* **121**, 160601 (2018).
- [46] L. L. Treffestädt and M. Schmidt, Universality in driven and equilibrium hard sphere liquid dynamics, *Phys. Rev. Lett.* **126**, 058002 (2021).
- [47] A. P. Antonov, A. Ryabov, and P. Maass, Solitons in overdamped Brownian dynamics, *Phys. Rev. Lett.* **129**, 080601 (2022).
- [48] J. Mattsson, H. M. Wyss, A. Fernandez-Nieves, K. Miyazaki, Z. Hu, D. R. Reichman, and D. A. Weitz, Soft colloids make strong glasses, *Nature (London)* **462**, 83 (2009).
- [49] D. T. N. Chen, Q. Wen, P. A. Janmey, J. C. Crocker, and A. G. Yodh, Rheology of soft materials, *Annu. Rev. Condens. Matter Phys.* **1**, 301 (2010).
- [50] Y. Han, Y. Shokef, A. M. Alsayed, P. Yunker, T. C. Lubensky, and A. G. Yodh, Geometric frustration in buckled colloidal monolayers, *Nature (London)* **456**, 898 (2008).
- [51] D. Zhou, F. Wang, B. Li, X. Lou, and Y. Han, Glassy spin dynamics in geometrically frustrated buckled colloidal crystals, *Phys. Rev. X* **7**, 021030 (2017).
- [52] S. Sacanna, W. T. M. Irvine, P. M. Chaikin, and D. J. Pine, Lock and key colloids, *Nature (London)* **464**, 575 (2010).
- [53] L. Feng, B. Laderman, S. Sacanna, and P. Chaikin, Re-entrant solidification in polymer-colloid mixtures as a consequence of competing entropic and enthalpic attractions, *Nat. Mater.* **14**, 61 (2015).
- [54] A. Rosato, K. J. Strandburg, F. Prinz, and R. H. Swendsen, Why the Brazil nuts are on top: Size segregation of particulate matter by shaking, *Phys. Rev. Lett.* **58**, 1038 (1987).
- [55] J. Duran, J. Rajchenbach, and E. Clément, Arching effect model for particle size segregation, *Phys. Rev. Lett.* **70**, 2431 (1993).
- [56] P. G. Bolhuis, A. A. Louis, and J.-P. Hansen, Influence of polymer-excluded volume on the phase-behavior of colloid-polymer mixtures, *Phys. Rev. Lett.* **89**, 128302 (2002).
- [57] Y. Pollak, S. Goldberg, and R. Amit, Self-avoiding wormlike chain model for double-stranded-DNA loop formation, *Phys. Rev. E* **90**, 052602 (2014).
- [58] W. Reisner, J. P. Beech, N. B. Larsen, H. Flyvbjerg, A. Kristensen, and J. O. Tegenfeldt, Nanoconfinement-enhanced conformational response of single DNA molecules to changes in ionic environment, *Phys. Rev. Lett.* **99**, 058302 (2007).
- [59] D. R. Tree, Y. Wang, and K. D. Dorfman, Extension of DNA in a nanochannel as a rod-to-coil transition, *Phys. Rev. Lett.* **110**, 208103 (2013).
- [60] A. P. Antonov, D. Voráč, A. Ryabov, and P. Maass, Collective excitations in jammed states: Ultrafast defect propagation and finite-size scaling, *New J. Phys.* **24**, 093020 (2022).
- [61] A. Carpio and L. L. Bonilla, Wave front depinning transition in discrete one-dimensional reaction-diffusion systems, *Phys. Rev. Lett.* **86**, 6034 (2001).
- [62] See Supplemental Material at <http://link.aps.org/supplemental/10.1103/PhysRevResearch.6.L012044> for two supplemental videos and one file to support the main results.
- [63] J. C. Crocker and D. G. Grier, Microscopic measurement of the pair interaction potential of charge-stabilized colloid, *Phys. Rev. Lett.* **73**, 352 (1994).
- [64] A. V. Straube, R. P. A. Dullens, L. Schimansky-Geier, and A. A. Louis, Zigzag transitions and nonequilibrium pattern formation in colloidal chains, *J. Chem. Phys.* **139**, 134908 (2013).
- [65] J. D. Weeks, D. Chandler, and H. C. Andersen, Role of repulsive forces in determining the equilibrium structure of simple liquids, *J. Chem. Phys.* **54**, 5237 (1971).
- [66] N. Tsapis, E. R. Dufresne, S. S. Sinha, C. S. Riera, J. W. Hutchinson, L. Mahadevan, and D. A. Weitz, Onset of buckling in drying droplets of colloidal suspensions, *Phys. Rev. Lett.* **94**, 018302 (2005).
- [67] F. Meng, M. Doi, and Z. Ouyang, Cavitation in drying droplets of soft matter solutions, *Phys. Rev. Lett.* **113**, 098301 (2014).
- [68] G. Munglani, F. K. Wittel, R. Vetter, F. Bianchi, and H. J. Herrmann, Collapse of orthotropic spherical shells, *Phys. Rev. Lett.* **123**, 058002 (2019).
- [69] X. Wang, L. Wu, G. Wang, and G. Chen, Dynamic crystallization and phase transition in evaporating colloidal droplets, *Nano Lett.* **19**, 8225 (2019).